A simple finite volume weighted essentially non-oscillatory schemes on triangular meshes[1]

Jun Zhu[2] and Jianxian Qiu[3]

Abstract

In this paper, we present a simple high order finite volume weighted essentially non-oscillatory (WENO) schemes to solve hyperbolic conservation laws on triangular meshes. The main advantages of these schemes presented in the paper are their compactness, robustness and could maintain good convergence property for solving steady state problems. Comparing with the classical finite volume WENO schemes [12], there are two major advantages of the new WENO schemes. The first, the associated optimal linear weights are independent on topological structure of meshes, can be any positive numbers with only requirement that their summation equals to one, and the second is that the new scheme is more compact and efficient than the scheme in [12]. Extensive numerical results are provided to illustrate the good performance of these new WENO schemes.

Key Words: weighted essentially non-oscillatory scheme, triangular mesh, finite volume method, high order accuracy, convergence property.

AMS(MOS) subject classification: 65M60, 35L65

[1]The research of J. Zhu is partly supported by NSFC grant 11372005 and the State Scholarship Fund of China for studying abroad, the research of J. Qiu is partly supported by NSAF grant U1630247 and NSFC grants 11571290.

[2]College of Science, Nanjing University of Aeronautics and Astronautics, Nanjing, Jiangsu 210016, P.R. China. E-mail: zhujun@nuaa.edu.cn.

[3]School of Mathematical Sciences and Fujian Provincial Key Laboratory of Mathematical Modeling and High-Performance Scientific Computing, Xiamen University, Xiamen, Fujian 361005, P. R. China. E-mail: jxqiu@xmu.edu.cn.

1 Introduction

In this paper, we study the high order finite volume numerical methods for solving the nonlinear hyperbolic conservation laws

$$\begin{cases} u_t + f(u)_x + g(u)_y = 0, \\ u(x, y, 0) = u_0(x, y), \end{cases} \tag{1.1}$$

on two dimensional triangular meshes. Essentially non-oscillatory (ENO) and weighted ENO (WENO) schemes are high order numerical methods for solving (1.1). ENO schemes were designed by Harten et al. [11, 22, 23]. The first WENO scheme was constructed by Liu, Osher and Chan for a third order finite volume version [15]. In 1996, third and fifth order finite difference WENO schemes were constructed by Jiang and Shu [13] in multi-space dimensions, with a general framework for the design of smoothness indicators and nonlinear weights. Some classical finite volume WENO schemes on unstructured and structured meshes were developed in [8, 12, 14, 17, 19]. Among them, a key point in WENO schemes is a linear combination of lower order fluxes or reconstruction to obtain a higher order approximation. Both ENO and WENO schemes use the idea of adaptive stencils to automatically achieve high order accuracy and non-oscillatory property nearby strong discontinuities. For the system case, such as Euler equations, WENO schemes based on local characteristic decompositions and flux splitting to avoid spurious oscillatory. Harten [9] first presented a two dimensional finite volume ENO schemes. Then Casper [3] and together with Atkins [4] studied the finite volume approach in developing multi-dimensional high order accurate ENO schemes for hyperbolic conservation laws. The most important and main framework of totally two dimensional finite volume WENO schemes on unstructured meshes were proposed by Hu and Shu [12]. In their paper, they proposed a third order WENO scheme by using a combination of nine linear polynomials and a fourth order WENO scheme by using a combination of six quadratic polynomials, gave a new way of measuring two dimensional smoothness of numerical solutions which are different to the expressions specified in [1] and [8]. But the skills of maintaining the positivity of linear weights for the third and fourth order finite

volume WENO schemes are too sophisticated to be fulfilled and such circumstance results in the lack of engineering applications as it was pointed out in [12]. Qiu and Shu gave a framework of totally two dimensional finite volume WENO schemes on structured meshes in [18], in which they expressed the construction principle of the linear weights in detail and the free parameters were then determined in a least squares sense so that the linear weights are unique and positive, and only depended on the geometries of computing meshes. After the analysis of the finite volume WENO schemes in the literature, generally speaking, there are two different kinds of the finite volume WENO schemes: one type of WENO schemes [6, 7, 8, 24] whose order of accuracy is not higher than that of the reconstruction on each smaller spatial stencils. Their nonlinear weights are artificially set as any positive numbers on condition that the summation is one for sustaining the conservative property without needing the maintaining of the order accuracy, except for keeping nonlinear stability and avoiding spurious oscillations robustly. The second type of WENO schemes [12, 19, 27] et al. whose order of accuracy is higher than that of the reconstruction on each smaller stencils. This type of WENO schemes is more difficult to construct mainly originates in solving linear systems for getting optimal linear weights, however, they could have a more compact spatial stencil than previous type of WENO schemes to achieve the same order accuracy in smooth region.

Based on these evaluations, in this paper, a class of new third order and fourth order finite volume WENO schemes which have all advantages and avoids drawbacks of two different types of WENO schemes are presented. The basic flowchart of third order WENO scheme is briefly narrated as follows. When we construct the third order finite volume WENO scheme, we adapt the idea of unequal size spatial stencils [32, 33], that is that we use a central big spatial stencil which contains at least six triangular cells including the target cell and its neighboring triangular cells to reconstruct a quadratic polynomial based on the information of conservative variables defined on each cell, and use four four-cell smaller stencils including the target cell and its neighboring cells to reconstruct four linear polynomials on the associ-

ated smaller spatial stencils in a least squares sense. And the quadratic polynomial needs to be modified by the subtraction of four linear polynomials with suitable parameters so as to keep third order approximations at Gaussian points on the boundaries of the target cell in smooth region [12, 21, 29]. Hereafter, any positive linear weights could be randomly chosen on condition that their summation equals to one. And we should keep a relative equilibrium between the sharp shock transitions and spurious oscillations in nonsmooth region. After computing the smoothness indicators and nonlinear weights, together with the third order TVD Runge-Kutta time discretization method [22], the new finite volume scheme is accomplished both in space and time. As analyzed in [16], Liu and Zhang found that it is hard to design a robust WENO scheme when facing distorted local mesh geometries or degenerate cases when the mesh quality varies for complex domain geometry because of the linear weights are negative greatly or inexistent at all, which would tremendously destroy finite volume WENO schemes' good performance such as high order accuracy, robustness and sharp shock transitions. Following the principles proposed by Sonar [20], Harten and Chakravarthy [10], and Vankeirsbilck [25], we find [12] violates the principles and a new layer of spatial cells are needed for constructing the fourth order finite volume WENO scheme [31], and three six-cell spatial stencils are added in the reconstruction procedures. So the new fourth order finite volume WENO scheme in comparison with [12, 31], is more compact, robust, needs only five spatial stencils and abides by the procedures as specified in constructing the new third order finite volume WENO scheme without considering the topological structure of the computational meshes once again.

The organization of the paper is as follows: in Section 2 and Section 3, we emphasize the principle of constructing the new third order and fourth order finite volume WENO schemes in detail. In Section 4, some numerical tests are presented to verify the simplicity and efficiency of these new finite volume schemes. Concluding remarks are given in Section 5.

2 Third order WENO scheme

We consider two dimensional conservation laws (1.1) on triangular meshes and integrate (1.1) over the target cell $\triangle_0$ to obtain the semi-discrete finite volume formula as

$$\frac{d\bar{u}_0(t)}{dt} = -\frac{1}{|\triangle_0|}\int_{\partial\triangle_0} F\cdot\vec{n}ds = L(u), \tag{2.1}$$

where $\bar{u}_0(t) = \frac{1}{|\triangle_0|}\int_{\triangle_0} u(x,y,t)dxdy$, $F = (f,g)^T$, $\partial\triangle_0$ is the boundary of the target cell $\triangle_0$ which is composed of three edges (line segments), $|\triangle_0|$ is the area of the target cell $\triangle_0$ and $\vec{n}$ denotes the outward unit normal to the edge of the target cell. The line integrals in (2.1) are discretized by a two-point Gaussian integration formula [12] on every edge (for example, for a line segment with two endpoints (x_1,y_1) and (x_2,y_2), the two-point Gaussian quadrature points are $(x_{G_1},y_{G_1}) = ((\frac{1}{2}+\frac{\sqrt{3}}{6})x_1+(\frac{1}{2}-\frac{\sqrt{3}}{6})x_2, (\frac{1}{2}+\frac{\sqrt{3}}{6})y_1+(\frac{1}{2}-\frac{\sqrt{3}}{6})y_2)$ and $(x_{G_2},y_{G_2}) = ((\frac{1}{2}-\frac{\sqrt{3}}{6})x_1+(\frac{1}{2}+\frac{\sqrt{3}}{6})x_2, (\frac{1}{2}-\frac{\sqrt{3}}{6})y_1+(\frac{1}{2}+\frac{\sqrt{3}}{6})y_2)$, and the associated Gaussian quadrature weights are $\sigma_1=\sigma_2=\frac{1}{2}$):

$$\int_{\partial\triangle_0} F\cdot\vec{n}ds \approx \sum_{\ell\ell=1}^{3}|\partial\triangle_{0_{\ell\ell}}|\sum_{\ell=1}^{2}\sigma_\ell F(u(x_{G_{\ell\ell_\ell}},y_{G_{\ell\ell_\ell}},t))\cdot\vec{n}_{\ell\ell}. \tag{2.2}$$

And $F(u(x_{G_{\ell\ell_\ell}},y_{G_{\ell\ell_\ell}},t))\cdot\vec{n}_{\ell\ell}$, $\ell=1,2$, $\ell\ell=1,2,3$, are reformulated by numerical fluxes such as the Lax-Friedrichs flux

$$\begin{aligned} F(u(x_{G_{\ell\ell_\ell}},y_{G_{\ell\ell_\ell}},t))\cdot\vec{n}_{\ell\ell} \approx \frac{1}{2}[(F(u^+(x_{G_{\ell\ell_\ell}},y_{G_{\ell\ell_\ell}},t))+F(u^-(x_{G_{\ell\ell_\ell}},y_{G_{\ell\ell_\ell}},t)))\cdot\vec{n}_{\ell\ell}- \\ \alpha(u^+(x_{G_{\ell\ell_\ell}},y_{G_{\ell\ell_\ell}},t)-u^-(x_{G_{\ell\ell_\ell}},y_{G_{\ell\ell_\ell}},t))], \ell=1,2, \ell\ell=1,2,3, \end{aligned} \tag{2.3}$$

in which α is taken as an upper bound for the eigenvalues of the Jacobian in the $\vec{n}_{\ell\ell}$ direction, and u_*^+ and u_*^- are the conservative values of u inside and outside of the boundaries of the target triangular cell (inside of the neighboring triangular cell) at different Gaussian points and $|\partial\triangle_{0_{\ell\ell}}|, \ell\ell=1,2,3$, are the length of the line segments. We then emphasize the procedures of a new third order finite volume WENO scheme on triangular meshes as follows and omit variable t if not cause confusion, unless specified otherwise. For simplicity, we relabel the reconstruction stencils which are shown in Figure 2.1.

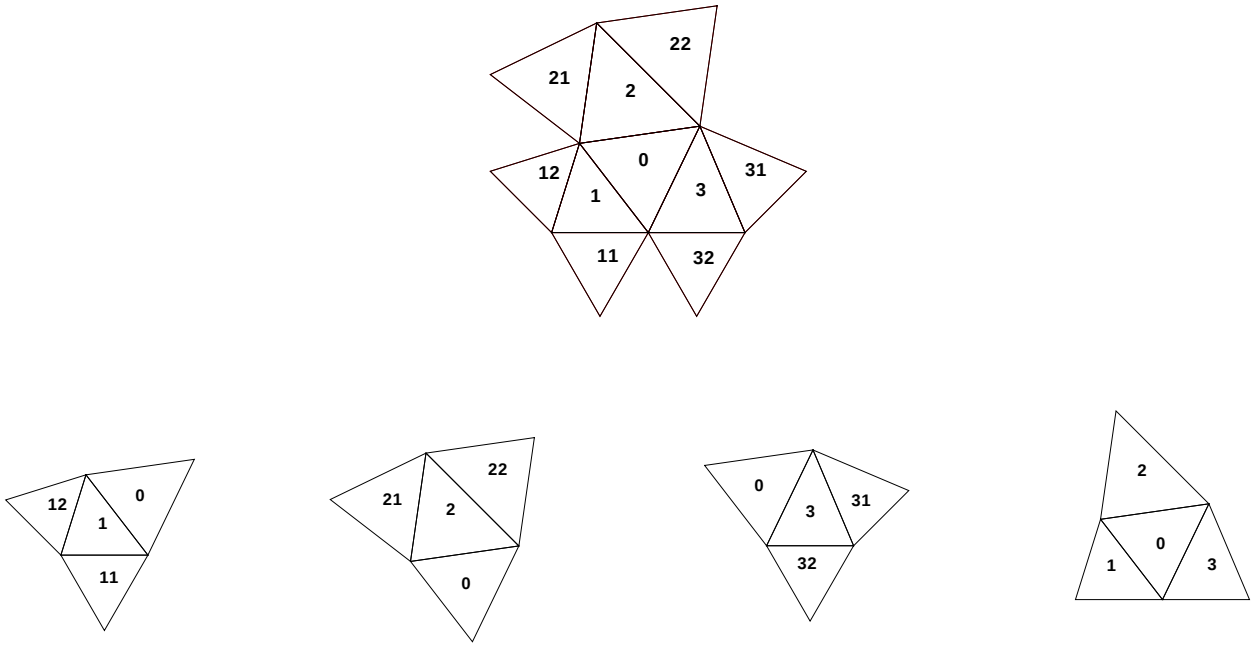

Figure 2.1: The typical stencils. From top to bottom and left to right: T_1, T_2, T_3, T_4, T_5.

The reconstruction of function $u(x, y, t)$ at different Gaussian quadrature points $(x_{G_{\ell\ell_\ell}}, y_{G_{\ell\ell_\ell}})$, $\ell = 1, 2$, $\ell\ell = 1, 2, 3$, on the boundaries of target cell $\triangle_0$ is narrated as follows.

Step 1.1. Select the big stencil as $T_1 = \{\triangle_0, \triangle_1, \triangle_2, \triangle_3, \triangle_{11}, \triangle_{12}, \triangle_{21}, \triangle_{22}, \triangle_{31}, \triangle_{32}\}$. Then we construct a quadratic polynomial $p_1(x, y) \in \{1, \frac{x-x_0}{|\triangle_0|^{\frac{1}{2}}}, \frac{y-y_0}{|\triangle_0|^{\frac{1}{2}}}, \frac{(x-x_0)^2}{|\triangle_0|}, \frac{(x-x_0)(y-y_0)}{|\triangle_0|}, \frac{(y-y_0)^2}{|\triangle_0|}\}$ on T_1 to obtain a third order approximation of conservative variable u and (x_0, y_0) is the barycenter of the target cell $\triangle_0$. Such quadratic polynomial has the same cell average of u on the target cell $\triangle_0$, and matches the cell averages of u on the other triangles in the set $T_1 \setminus \{\triangle_0\}$ in a least square sense [12]:

$$\frac{1}{|\triangle_0|}\int_{\triangle_0} p_1(x, y)dxdy = \bar{u}_0, \tag{2.4}$$

and

$$\min \sum_{\ell\in A}(\frac{1}{|\triangle_\ell|}\int_{\triangle_\ell} p_1(x, y)dxdy - \bar{u}_\ell)^2, A = \{1, 2, 3, 11, 12, 21, 22, 31, 32\}. \tag{2.5}$$

Step 1.2. Construct four linear polynomials $p_i(x, y) \in \{1, \frac{x-x_0}{|\triangle_0|^{\frac{1}{2}}}, \frac{y-y_0}{|\triangle_0|^{\frac{1}{2}}}\}$, $i = 2, 3, 4, 5$, which satisfy the cell average of the conservative variable u on the target cell $\triangle_0$ and match

the cell averages of u on the other triangles in a least square sense [12].

For the reconstruction of polynomial $p_2(x,y)$ defined on small stencil $T_2 = \{\triangle_0, \triangle_1, \triangle_{11}, \triangle_{12}\}$, it requires

$$\frac{1}{|\triangle_0|}\int_{\triangle_0} p_2(x,y)dxdy = \bar{u}_0, \tag{2.6}$$

and

$$\min \sum_{\ell\in A}(\frac{1}{|\triangle_\ell|}\int_{\triangle_\ell} p_2(x,y)dxdy - \bar{u}_\ell)^2,\ A = \{1,11,12\}. \tag{2.7}$$

For the reconstruction of polynomial $p_3(x,y)$ defined on small stencil $T_3 = \{\triangle_0, \triangle_2, \triangle_{21}, \triangle_{22}\}$, it requires

$$\frac{1}{|\triangle_0|}\int_{\triangle_0} p_3(x,y)dxdy = \bar{u}_0, \tag{2.8}$$

and

$$\min \sum_{\ell\in A}(\frac{1}{|\triangle_\ell|}\int_{\triangle_\ell} p_3(x,y)dxdy - \bar{u}_\ell)^2, A = \{2,21,22\}. \tag{2.9}$$

For the reconstruction of polynomial $p_4(x,y)$ defined on small stencil $T_4 = \{\triangle_0, \triangle_3, \triangle_{31}, \triangle_{32}\}$, it requires

$$\frac{1}{|\triangle_0|}\int_{\triangle_0} p_4(x,y)dxdy = \bar{u}_0, \tag{2.10}$$

and

$$\min \sum_{\ell\in A}(\frac{1}{|\triangle_\ell|}\int_{\triangle_\ell} p_4(x,y)dxdy - \bar{u}_\ell)^2, A = \{3,31,32\}. \tag{2.11}$$

For the reconstruction of polynomial $p_5(x,y)$ defined on small stencil $T_5 = \{\triangle_0, \triangle_1, \triangle_2, \triangle_3\}$, it requires

$$\frac{1}{|\triangle_0|}\int_{\triangle_0} p_5(x,y)dxdy = \bar{u}_0, \tag{2.12}$$

and

$$\min \sum_{\ell\in A}(\frac{1}{|\triangle_\ell|}\int_{\triangle_\ell} p_5(x,y)dxdy - \bar{u}_\ell)^2, A = \{1,2,3\}. \tag{2.13}$$

Remarks: We could also design three more compact linear polynomials defined on different three-cell stencils ($T_2 = \{\triangle_0, \triangle_1, \triangle_2\}$, $T_3 = \{\triangle_0, \triangle_2, \triangle_3\}$ and $T_4 = \{\triangle_0, \triangle_3, \triangle_1\}$) in comparison to the linear polynomials defined on four-cell smaller stencils (see Figure 2.1). By doing so, the reconstruction procedures violate the sectorial searching principle [10, 20, 25] and sometimes cause the computations to break down, for example, the blast wave problem and a Mach 3 wind tunnel with a step problem [26]. Based on such analysis and computation, we abandon the more compact three-cell stencils and fall back on the usage of the wider scale four-cell stencils.

Step 1.3. Define the values of the linear weights which are based on a balance between the sharp shock transitions and essentially nonoscillatory property in nonsmooth region. In this paper, following the practice in [6, 28], for example, one type of these linear weights which is applied in this paper is defined as γ_1=0.96, γ_2=0.01, γ_3=0.01, γ_4=0.01 and γ_5=0.01. We would like to claim that the choice principle of the linear weights is random and the linear weights could be any positive constants in case their summation is one and would not pollute the new finite volume WENO scheme's optimal order of accuracy by the similar methodologies specified in [29] for finite difference high order WENO scheme. However, some other robust WENO type schemes based on the artificial definition of the linear weights often degrade their optimal numerical accuracy.

Step 1.4. Compute the smoothness indicators, denote by β_ℓ, $\ell = 1, \ldots, 5$, which measure how smooth the functions $p_\ell(x, y)$, $\ell = 1, \ldots, 5$, are in the target cell $\triangle_0$. The smaller these smoothness indicators, the smoother the functions are in the target cell. We use the same recipe for the smoothness indicators as in [12, 13]:

$$\beta_\ell = \sum_{|l|=1}^{r} \int_{\triangle_0} |\triangle_0|^{|l|-1} \left(\frac{\partial^{|l|}}{\partial x^{l_1} \partial y^{l_2}} p_\ell(x, y) \right)^2 dxdy, \ \ell = 1, \ldots, 5, \tag{2.14}$$

where $l = (l_1, l_2)$, $|l| = l_1 + l_2$. And for $\ell = 1$, $r = 2$; for $\ell = 2, 3, 4, 5$, $r = 1$. Their expansions in Taylor series at (x_0, y_0) are

$$\beta_1 = \left(\sum_{|l|=1} \left(\frac{\partial^{|l|}}{\partial x^{l_1} \partial y^{l_2}} u(x, y, t)|_{(x_0, y_0, t)} \right)^2 \right) |\triangle_0|(1 + O(|\triangle_0|)) = O(|\triangle_0|), \tag{2.15}$$

and

$$\beta_\ell = \left(\sum_{|l|=1} \left(\frac{\partial^{|l|}}{\partial x^{l_1} \partial y^{l_2}} u(x,y,t)|_{(x_0,y_0,t)} \right)^2 \right) |\triangle_0|(1 + O(|\triangle_0|^{\frac{1}{2}})) = O(|\triangle_0|),\ \ell = 2,3,4,5. \tag{2.16}$$

Step 1.5. Compute the nonlinear weights based on the linear weights and the smoothness indicators. For instance, we use τ [29] which is simply defined as the absolute deference between β_1, β_2, β_3, β_4 and β_5, and is different to the formula specified in [2, 5]. The difference expansions in Taylor series at (x_0, y_0) are

$$\beta_1 - \beta_\ell = O(|\triangle_0|^{\frac{3}{2}}),\ \ell = 2,3,4,5. \tag{2.17}$$

Then,

$$\tau = \left(\frac{|\beta_1 - \beta_2| + |\beta_1 - \beta_3| + |\beta_1 - \beta_4| + |\beta_1 - \beta_5|}{4} \right)^2 = O(|\triangle_0|^3). \tag{2.18}$$

Then the associate nonlinear weights are defined as

$$\omega_\ell = \frac{\bar{\omega}_\ell}{\sum_{\ell\ell=1}^{5} \bar{\omega}_{\ell\ell}}, \qquad \bar{\omega}_\ell = \gamma_\ell (1 + \frac{\tau}{\varepsilon + \beta_\ell}), \quad \ell = 1,2,3,4,5. \tag{2.19}$$

Here ε is a small positive number to avoid the denominator of (2.19) to become zero. By the implementation of (2.18) in the smooth region, it satisfies

$$\frac{\tau}{\varepsilon + \beta_\ell} = O(|\triangle_0|^2), \ell = 1,2,3,4,5, \tag{2.20}$$

on condition that $\varepsilon \ll \beta_\ell$. Therefore, the nonlinear weights ω_ℓ, $\ell = 1,2,3,4,5$, satisfy the order accuracy condition $\omega_\ell = \gamma_\ell + O(|\triangle_0|)$ [2, 5], providing the third order accuracy to the WENO scheme narrated in [13, 21]. We confine $\varepsilon = 10^{-6}$ in all simulations in this paper.

Step 1.6. The new final reconstruction formulations of conservative values $u(x,y,t)$ at different Gaussian quadrature points $(x_{G_{\ell\ell_\ell}}, y_{G_{\ell\ell_\ell}})$, $\ell = 1,2$, $\ell\ell = 1,2,3$, on different line segments of the boundaries of the target cell $\triangle_0$ are given by

$$\begin{aligned} u^-(x_{G_{\ell\ell_\ell}}, y_{G_{\ell\ell_\ell}}, t) &= \omega_1 (\frac{1}{\gamma_1} p_1(x_{G_{\ell\ell_\ell}}, y_{G_{\ell\ell_\ell}}) - \frac{\gamma_2}{\gamma_1} p_2(x_{G_{\ell\ell_\ell}}, y_{G_{\ell\ell_\ell}}) - \frac{\gamma_3}{\gamma_1} p_3(x_{G_{\ell\ell_\ell}}, y_{G_{\ell\ell_\ell}}) - \\ &\frac{\gamma_4}{\gamma_1} p_4(x_{G_{\ell\ell_\ell}}, y_{G_{\ell\ell_\ell}}) - \frac{\gamma_5}{\gamma_1} p_5(x_{G_{\ell\ell_\ell}}, y_{G_{\ell\ell_\ell}})) + \omega_2 p_2(x_{G_{\ell\ell_\ell}}, y_{G_{\ell\ell_\ell}}) + \omega_3 p_3(x_{G_{\ell\ell_\ell}}, y_{G_{\ell\ell_\ell}}) + \\ &\omega_4 p_4(x_{G_{\ell\ell_\ell}}, y_{G_{\ell\ell_\ell}}) + \omega_5 p_5(x_{G_{\ell\ell_\ell}}, y_{G_{\ell\ell_\ell}}),\ \ell = 1,2,\ \ell\ell = 1,2,3. \end{aligned} \tag{2.21}$$

Remarks: The first term of the right hand side of (2.21) serves an important role in our reconstruction. If (2.21) is currently stated as $\omega_1 p_1(x_{G_{\ell\ell_\ell}}, y_{G_{\ell\ell_\ell}}) + \omega_2 p_2(x_{G_{\ell\ell_\ell}}, y_{G_{\ell\ell_\ell}}) + \omega_3 p_3(x_{G_{\ell\ell_\ell}}, y_{G_{\ell\ell_\ell}}) + \omega_4 p_4(x_{G_{\ell\ell_\ell}}, y_{G_{\ell\ell_\ell}}) + \omega_5 p_5(x_{G_{\ell\ell_\ell}}, y_{G_{\ell\ell_\ell}})$, the new third order finite volume scheme would absolutely degrade its optimal order of accuracy from third order to second order and get larger quantities of absolute numerical errors in L^1 and L^∞ norms even in smooth region, on account of the crucial effectiveness of $p_l(x_{G_{\ell\ell_\ell}}, y_{G_{\ell\ell_\ell}})$, $l = 2, 3, 4, 5$, which are available in case their smoothness indicators are smaller in comparison to the one of the quadratic polynomial over the target cell $\triangle_0$ in smooth region. In consideration of such circumstance, it is convincing for us to use (2.21) as a substitutive formulation. By performing such new formula, it is not very essential to precisely select the optimal linear weights for the sake of keeping third order accuracy in smooth region simultaneously maintaining the strong shocks and contact discontinuities sharply in nonsmooth region.

Step 1.7. Then the third order TVD Runge-Kutta time discretization method [22]

$$\begin{cases} u^{(1)} = u^n + \triangle t L(u^n), \\ u^{(2)} = \frac{3}{4}u^n + \frac{1}{4}u^{(1)} + \frac{1}{4}\triangle t L(u^{(1)}), \\ u^{n+1} = \frac{1}{3}u^n + \frac{2}{3}u^{(2)} + \frac{2}{3}\triangle t L(u^{(2)}), \end{cases} \tag{2.22}$$

is used to solve (2.1) and we could obtain fully discrete scheme both in space and time on triangular meshes.

Remarks: In the case that the cells in the big stencil are less than six for that some triangles are merged, we should use triangular cells in the next layer to guarantee information enough to reconstruct the quadratic polynomial in the least squares. There are two major differences between the reconstruction procedures for the third order finite volume WENO in this paper and in [12]. The first is that a big stencil and four small stencils are used in the paper, in the [12] a big stencil and nine small stencils are used. The second is that the linear weights are independent on geometry structure of meshes and can be any positive numbers with only requirement that their summation equals to one, and in the [12], the linear weights are depended on both geometry structure of meshes and where the value is reconstructed. If the quadrature points are not chosen properly or the geometry of the

computational meshes is rigid, the linear weights in [12] may become negative or even not exist at all [16, 19]. So the flowchart specified in this paper for narrating the new third finite volume WENO scheme is very simple and robust in setting different types of linear weights at any quadrature points, simultaneously keeping third order accuracy in smooth region without adjusting many parameters in constructing numerical schemes.

3 Fourth order WENO scheme

In this section, the procedures of a new fourth order finite volume WENO scheme on triangular meshes are specified. We use the same reconstruction stencils which are shown in Figure 2.1.

The reconstruction of function $u(x, y, t)$ at different Gaussian quadrature points $(x_{G_{\ell\ell_\ell}}, y_{G_{\ell\ell_\ell}})$, $\ell = 1, 2$, $\ell\ell = 1, 2, 3$, on the boundaries of target cell $\triangle_0$ is narrated as follows.

Step 2.1. Select the big stencil as $T_1 = \{\triangle_0, \triangle_1, \triangle_2, \triangle_3, \triangle_{11}, \triangle_{12}, \triangle_{21}, \triangle_{22}, \triangle_{31}, \triangle_{32}\}$. Then we construct a cubic polynomial $p_1(x, y) \in \{1, \frac{x-x_0}{|\triangle_0|^{\frac{1}{2}}}, \frac{y-y_0}{|\triangle_0|^{\frac{1}{2}}}, \frac{(x-x_0)^2}{|\triangle_0|}, \frac{(x-x_0)(y-y_0)}{|\triangle_0|}, \frac{(y-y_0)^2}{|\triangle_0|}, \frac{(x-x_0)^3}{|\triangle_0|^{\frac{3}{2}}}, \frac{(x-x_0)^2(y-y_0)}{|\triangle_0|^{\frac{3}{2}}}, \frac{(x-x_0)(y-y_0)^2}{|\triangle_0|^{\frac{3}{2}}}, \frac{(y-y_0)^3}{|\triangle_0|^{\frac{3}{2}}}\}$ on T_1 to obtain a fourth order approximation of conservative variable u by requiring that it has the same cell averages of u on the target cell $\triangle_0$ and the other triangles:

$$\frac{1}{|\triangle_\ell|}\int_{\triangle_\ell} p_1(x, y)dxdy = \bar{u}_\ell, \ell = 0, 1, 2, 3, 11, 12, 21, 22, 31, 32. \tag{3.1}$$

Step 2.2. Construct four linear polynomials $p_i(x, y) \in \{1, \frac{x-x_0}{|\triangle_0|^{\frac{1}{2}}}, \frac{y-y_0}{|\triangle_0|^{\frac{1}{2}}}\}$, $i = 2, 3, 4, 5$, which satisfy the cell average of the conservative variable u on the target cell $\triangle_0$ and match the cell averages of u on the other triangles in a least square sense [12], which are identical to that specified in Step 1.2 and thus omitted here for simplicity.

Remarks: For the purpose of constructing a new fourth order finite volume WENO scheme, we need to construct a cubic polynomial which has ten degrees of freedom based on the big central spatial stencil for causing less truncation errors than on the big biased spatial stencil. We only consider the case where $\triangle_\ell, \ell = 0, ..., 32$, are distinct in the big stencil (see

Figure 2.1). We construct the cubic polynomial $p_1(x, y)$ by requiring that it has the same cell averages on triangular cells including $\triangle_0$ and its neighboring three cells and their next six neighboring cells in T_1. It seems that for most computational meshes this reconstruction circumstance is enough, otherwise, the next layer of triangular cells are searched and the associated cubic polynomial is reconstructed in a least square sense if necessary. If a cubic polynomial and nine linear polynomials specified in [12] are reconstructed, the linear systems for solving the linear weights at different quadrature points are grossly overdetermined and insoluble. So the fourth order finite volume WENO scheme on triangular meshes is being less in this way. So as to remedy this drawback, Hu and Shu [12] used a cubic polynomial based on the cell averages defined on a ten-cell spatial stencil and six quadratic polynomials based on the cell averages defined on six six-cell smaller spatial stencils and compute linear systems on different quadrature points for the sake of getting the linear weights which reveal the relationship between the cubic polynomial and associated six quadratic polynomials at different quadrature points. This methodology is very essential for the second type of finite volume WENO schemes to obtain their optimal order accuracy in smooth region on condition that the geometry meshes not distort too much, otherwise, we apply the technique of treating negative weights in WENO scheme [19] or the technique of achieving a robust unstructured finite volume WENO reconstruction on complex mesh geometries [16].

Step 2.3. Define the values of the linear weights as γ_1=0.96, γ_2=0.01, γ_3=0.01, γ_4=0.01 and γ_5=0.01.

Step 2.4. Compute the smoothness indicators, denote by β_ℓ, $\ell = 1, \ldots, 5$, [12, 13] by the application of (2.14). Their expansions in Taylor series at (x_0, y_0) are

$$\beta_1 = \left(\sum_{|l|=1} (\frac{\partial^{|l|}}{\partial x^{l_1} \partial y^{l_2}} u(x, y, t)|_{(x_0,y_0,t)})^2 \right) |\triangle_0|(1 + O(|\triangle_0|^{\frac{3}{2}})) = O(|\triangle_0|), \tag{3.2}$$

and

$$\beta_\ell = \left(\sum_{|l|=1} (\frac{\partial^{|l|}}{\partial x^{l_1} \partial y^{l_2}} u(x, y, t)|_{(x_0,y_0,t)})^2 \right) |\triangle_0|(1 + O(|\triangle_0|^{\frac{1}{2}})) = O(|\triangle_0|), \ \ell = 2, 3, 4, 5. \tag{3.3}$$

Step 2.5. Compute the nonlinear weights based on the linear weights and the smoothness indicators. For instance, we use τ [29] which is simply defined as the absolute deference between β_1, β_2, β_3, β_4 and β_5, and the difference expansions in Taylor series at (x_0, y_0) are

$$\beta_1 - \beta_\ell = O(|\triangle_0|^{\frac{3}{2}}),\ \ell = 2, 3, 4, 5. \tag{3.4}$$

So it satisfies

$$\tau = (\frac{|\beta_1 - \beta_2| + |\beta_1 - \beta_3| + |\beta_1 - \beta_4| + |\beta_1 - \beta_5|}{4})^2 = O(|\triangle_0|^3). \tag{3.5}$$

Then the associate nonlinear weights are defined as in Step 1.5. By the performance of (3.5) in the smooth region, it satisfies

$$\frac{\tau}{\varepsilon + \beta_\ell} = O(|\triangle_0|^2), \ell = 1, 2, 3, 4, 5, \tag{3.6}$$

on condition that $\varepsilon \ll \beta_\ell$. Therefore, the nonlinear weights ω_ℓ, $\ell = 1, 2, 3, 4, 5$, satisfy the order accuracy condition $\omega_\ell = \gamma_\ell + O(|\triangle_0|^{\frac{3}{2}})$ [2, 5], providing the fourth order accuracy to the WENO scheme [13, 21].

Step 2.6. The new final reconstruction formulations of conservative values $u(x, y, t)$ at different Gaussian quadrature points $(x_{G_{\ell\ell_\ell}}, y_{G_{\ell\ell_\ell}})$, $\ell = 1, 2$, $\ell\ell = 1, 2, 3$, on different line segments of the boundaries of the target cell $\triangle_0$ are given by (2.21).

Step 2.7. Then the third order TVD Runge-Kutta time discretization method [22] (2.22) is applied for solving the ODE (2.1) on triangular meshes.

Remarks: In [20], Sonar pointed out the constructional principle of essentially non-oscillatory finite volume approximations to compressible fluid dynamics on triangular cells. He gave a new narration of applicable methodologies for the stencil selection principle to recover polynomials of arbitrary degree. Harten and Chakravarthy [10] proposed a sectorial search in order to keep the number of possible stencils small. Sectorial search was also used by Vankeirsbilck [25] in connection with a box method. So it is reasonable to search for bigger spatial stencil including sixteen cells [31] and reconstruct a cubic polynomial in a least square sense and nine quadratic polynomials, and calculate linear systems for solving

linear weights at different quadrature points. And this analysis partly explains the truth why there is no the fourth order WENO scheme for the simulation of a Mach 3 wind tunnel with a step problem in [12] because of the violation of the associated principles. Generally speaking, it is the first time for us to design a fourth order finite volume WENO scheme by the usage of the cell averages on only ten cells to formulate five unequal degree polynomials for high order approximations at different quadrature points robustly simultaneously without taking into account the good or bad quality of the computational meshes.

4 Numerical results

In this section we provide numerical results to demonstrate the performance of the new third order and fourth order finite volume WENO schemes on triangular meshes described in section 2 and section 3. For systems of the compressible Euler equations, all of the reconstructions are performed in the local characteristic directions to avoid spurious oscillations. For the purpose of evaluating whether the random choice of the linear weights would pollute the optimal order accuracy of these new WENO schemes or not, we set four different types of linear weights in the numerical accuracy cases as: (1) γ_1=0.96, γ_2=0.01, γ_3=0.01, γ_4=0.01 and γ_5=0.01; (2) γ_1=0.2, γ_2=0.2, γ_3=0.2, γ_4=0.2 and γ_5=0.2; (3) γ_1=0.01, γ_2=0.2475, γ_3=0.2475, γ_4=0.2475 and γ_5=0.2475; (4) γ_1=0.01, γ_2=0.01, γ_3=0.01, γ_4=0.01 and γ_5=0.96. And then we recover γ_1=0.96, $\gamma_2 = \gamma_3 = \gamma_4 = \gamma_5$=0.01 in the latter examples, unless specified otherwise.

Example 4.1. We solve the following nonlinear scalar Burgers equation in two dimensions

$$\mu_t + (\frac{\mu^2}{2})_x + (\frac{\mu^2}{2})_y = 0, (x, y) \in [-2, 2] \times [-2, 2], \tag{4.1}$$

with the initial condition $\mu(x, y, 0) = 0.5 + \sin(\pi(x + y)/2)$ and periodic boundary conditions in both directions. We compute the solution up to $t = 0.5/\pi$. For this test case, the sample of the computational mesh is shown in Figure 4.1. The errors and numerical orders of accuracy for the third order and fourth order finite volume WENO schemes are shown in Table 4.1.

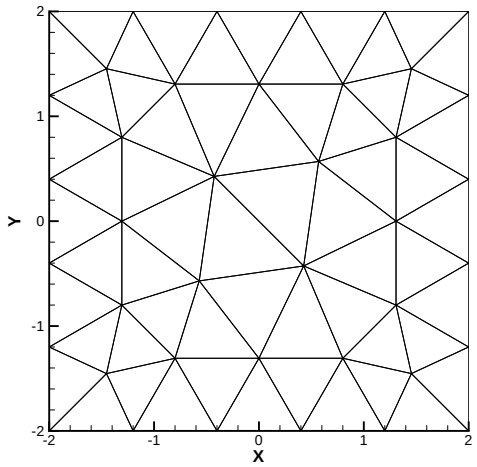

Figure 4.1: Burgers equation. Sample mesh.

The new finite volume WENO schemes can keep the designed order of accuracy with different sets of linear weights in this classical scalar nonlinear accuracy test case.

Example 4.2. We solve the two dimensional Euler equations

$$\frac{\partial}{\partial t}\begin{pmatrix}\rho\\ \rho\mu\\ \rho\nu\\ E\end{pmatrix}+\frac{\partial}{\partial x}\begin{pmatrix}\rho\mu\\ \rho\mu^2+p\\ \rho\mu\nu\\ \mu(E+p)\end{pmatrix}+\frac{\partial}{\partial y}\begin{pmatrix}\rho\nu\\ \rho\nu\mu\\ \rho\nu^2+p\\ \nu(E+p)\end{pmatrix}=0,(x,y)\in[0,2]\times[0,2]. \quad (4.2)$$

In which ρ is density; μ and ν are the velocities in the x and y directions, respectively; E is total energy; and p is pressure, which is related to the total energy by $E = p/(\gamma-1)+\frac{1}{2}(\rho(\mu^2+\nu^2)$ with $\gamma = 1.4$. The initial conditions are: $\rho(x,y,0) = 1+0.2\sin(\pi(x+y))$, $\mu(x,y,0) = 0.5$, $\nu(x,y,0) = 0.5$, $p(x,y,0) = 1$. Periodic boundary conditions are applied in both directions. The exact solution is $\rho(x,y,t) = 1+0.2\sin(\pi(x+y-t))$. The solution is computed up to $t = 2$. For this test case the sample mesh is shown in Figure 4.2. The errors and numerical orders of the third order and fourth order WENO schemes are shown in Table 4.2. We can see that these schemes again keep the theoretical order of accuracy with different artificially chosen linear weights.

Example 4.3. We solve the two dimensional Euler equations (4.2) with the Riemann initial condition for the Lax problem:

$$(\rho,\mu,\nu,p)^T=\begin{cases}(0.445,0.698,0,3.528)^T, & x\in[-0.5,0),\\ (0.5,0,0,0.571)^T, & x\in[0,0.5].\end{cases} \quad (4.3)$$

Table 4.1: $\mu_t + \left(\frac{\mu^2}{2}\right)_x + \left(\frac{\mu^2}{2}\right)_y = 0$. $\mu(x, y, 0) = 0.5 + \sin(\pi(x + y)/2)$. Periodic boundary conditions in both directions. $T = 0.5/\pi$. L^1 and L^∞ errors. WENO schemes.

	WENO3 (1)				WENO3 (2)			
h	L^1 error	order	L^∞ error	order	L^1 error	order	L^∞ error	order
4/5	3.84E-2		1.32E-1		5.85E-2		2.00E-1	
4/10	8.71E-3	2.14	4.92E-2	1.43	1.41E-2	2.05	8.38E-2	1.26
4/20	1.36E-3	2.67	1.19E-2	2.04	1.42E-3	3.31	1.18E-2	2.82
4/40	2.08E-4	2.71	2.18E-3	2.45	2.07E-4	2.78	2.18E-3	2.44
4/80	2.84E-5	2.87	3.07E-4	2.83	2.84E-5	2.87	3.07E-4	2.83
	WENO3 (3)				WENO3 (4)			
h	L^1 error	order	L^∞ error	order	L^1 error	order	L^∞ error	order
4/5	6.04E-2		2.04E-1		3.93E-2		1.51E-1	
4/10	1.50E-2	2.00	8.71E-2	1.23	9.03E-3	2.12	4.97E-2	1.61
4/20	1.45E-3	3.37	1.18E-2	2.88	1.37E-3	2.72	1.19E-2	2.06
4/40	2.07E-4	2.81	2.18E-3	2.44	2.08E-4	2.72	2.18E-3	2.45
4/80	2.84E-5	2.86	3.07E-4	2.83	2.84E-5	2.87	3.07E-4	2.83
	WENO4 (1)				WENO4 (2)			
h	L^1 error	order	L^∞ error	order	L^1 error	order	L^∞ error	order
4/5	3.68E-2		1.54E-1		9.35E-2		2.80E-1	
4/10	3.59E-3	3.36	3.78E-2	2.03	1.89E-2	2.30	1.08E-1	1.36
4/20	1.51E-4	4.56	1.82E-3	4.38	9.97E-4	4.25	1.68E-2	2.70
4/40	7.08E-6	4.42	1.20E-4	3.91	1.69E-5	5.88	4.37E-4	5.26
4/80	3.25E-7	4.44	7.48E-6	4.01	3.76E-7	5.49	7.48E-6	5.87
	WENO4 (3)				WENO4 (4)			
h	L^1 error	order	L^∞ error	order	L^1 error	order	L^∞ error	order
4/5	9.65E-2		2.87E-1		4.01E-2		1.62E-1	
4/10	2.05E-2	2.23	1.12E-1	1.35	6.20E-3	2.69	4.05E-2	2.00
4/20	1.19E-3	4.11	1.89E-2	2.57	2.70E-4	4.52	4.77E-3	3.08
4/40	1.94E-5	5.94	5.33E-4	5.15	8.55E-6	4.98	1.20E-4	5.31
4/80	3.92E-7	5.63	7.48E-6	6.15	3.27E-7	4.70	7.48E-6	4.00

Table 4.2: 2D Euler equations: initial data $\rho(x,y,0) = 1 + 0.2\sin(\pi(x+y))$, $\mu(x,y,0) = 0.5$, $\nu(x,y,0) = 0.5$, and $p(x,y,0) = 1$. Periodic boundary conditions in both directions. $T = 2.0$. L^1 and L^∞ errors. WENO schemes.

	WENO3 (1)				WENO3 (2)			
h	L^1 error	order	L^∞ error	order	L^1 error	order	L^∞ error	order
2/5	1.09E-1		1.73E-1		1.09E-1		1.73E-1	
2/10	3.98E-2	1.45	7.30E-2	1.25	4.05E-2	1.43	7.51E-2	1.21
2/20	6.59E-3	2.60	1.41E-2	2.37	6.60E-3	2.62	1.43E-2	2.39
2/40	8.49E-4	2.96	1.81E-3	2.97	8.49E-4	2.96	1.81E-3	2.98
2/80	1.04E-4	3.03	2.19E-4	3.04	1.04E-4	3.03	2.19E-4	3.04
	WENO3 (3)				WENO3 (4)			
h	L^1 error	order	L^∞ error	order	L^1 error	order	L^∞ error	order
2/5	1.09E-1		1.73E-1		1.09E-1		1.73E-1	
2/10	4.06E-2	1.43	7.56E-2	1.20	3.99E-2	1.45	7.33E-2	1.24
2/20	6.60E-3	2.62	1.43E-2	2.40	6.59E-3	2.60	1.41E-2	2.37
2/40	8.49E-4	2.96	1.81E-3	2.98	8.49E-4	2.96	1.81E-3	2.97
2/80	1.04E-4	3.03	2.19E-4	3.04	1.04E-4	3.03	2.19E-4	3.04
	WENO4 (1)				WENO4 (2)			
h	L^1 error	order	L^∞ error	order	L^1 error	order	L^∞ error	order
2/5	2.98E-2		5.86E-2		6.41E-2		1.09E-1	
2/10	1.10E-3	4.75	4.43E-3	3.73	3.16E-3	4.34	1.82E-2	2.59
2/20	4.43E-5	4.64	2.06E-4	4.42	1.06E-4	4.90	1.08E-3	4.07
2/40	1.93E-6	4.52	9.08E-6	4.51	2.14E-6	5.63	1.34E-5	6.34
2/80	9.80E-8	4.30	4.76E-7	4.25	9.80E-8	4.45	4.91E-7	4.77
	WENO4 (3)				WENO4 (4)			
h	L^1 error	order	L^∞ error	order	L^1 error	order	L^∞ error	order
2/5	6.74E-2		1.13E-1		3.45E-2		6.89E-2	
2/10	3.72E-3	4.18	2.09E-2	2.44	1.20E-3	4.84	6.65E-3	3.37
2/20	1.27E-4	4.86	1.28E-3	4.03	4.74E-5	4.67	3.44E-4	4.27
2/40	2.23E-6	5.84	1.54E-5	6.38	1.92E-6	4.62	9.07E-6	5.25
2/80	9.81E-8	4.51	4.95E-7	4.96	9.79E-8	4.30	4.78E-7	4.24

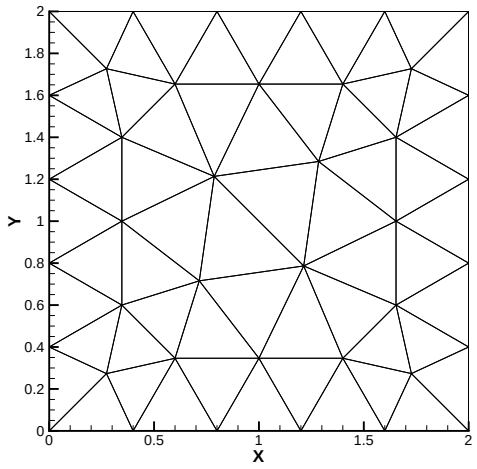

Figure 4.2: 2D Euler equations. Sample mesh.

For $t = 0.16$, we present in Figure 4.3 the exact solution and the computed density ρ obtained with the new third order and fourth order finite volume WENO schemes. These two dimensional triangular WENO schemes are applied to this one dimensional shock tube problem. The solution of the Euler equations (4.2) in the domain of $[-0.5, 0.5]\times[-5\triangle x, 5\triangle x]$ with a triangulation of 101 vertices in the x direction and 11 vertices in the y direction. The periodic boundary condition is applied in the y direction. The results and zoomed in picture for two different schemes are shown in Figure 4.3. We observe that the computational results obtained by the associated WENO schemes are good.

Example 4.4. We solve the two dimensional Euler equations (4.2) with Riemann initial condition for the Sod problem:

$$(\rho, \mu, \nu, p)^T = \begin{cases} (1, 0, 0, 2.5)^T, & x \in [-5, 0), \\ (0.125, 0, 0, 0.25)^T, & x \in [0, 5]. \end{cases} \tag{4.4}$$

For $t = 2$, we present in Figure 4.4 the exact solution and the computed density ρ obtained with the new third order and fourth order finite volume WENO schemes. The solution of the Euler equations (4.2) in the domain of $[-5, 5] \times [-5\triangle x, 5\triangle x]$ with a triangulation of 101 vertices in the x direction and 11 vertices in the y direction. The periodic boundary condition is applied in the y direction. The results and zoomed in picture for associated schemes are shown in Figure 4.4. The numerical results computed by the WENO schemes

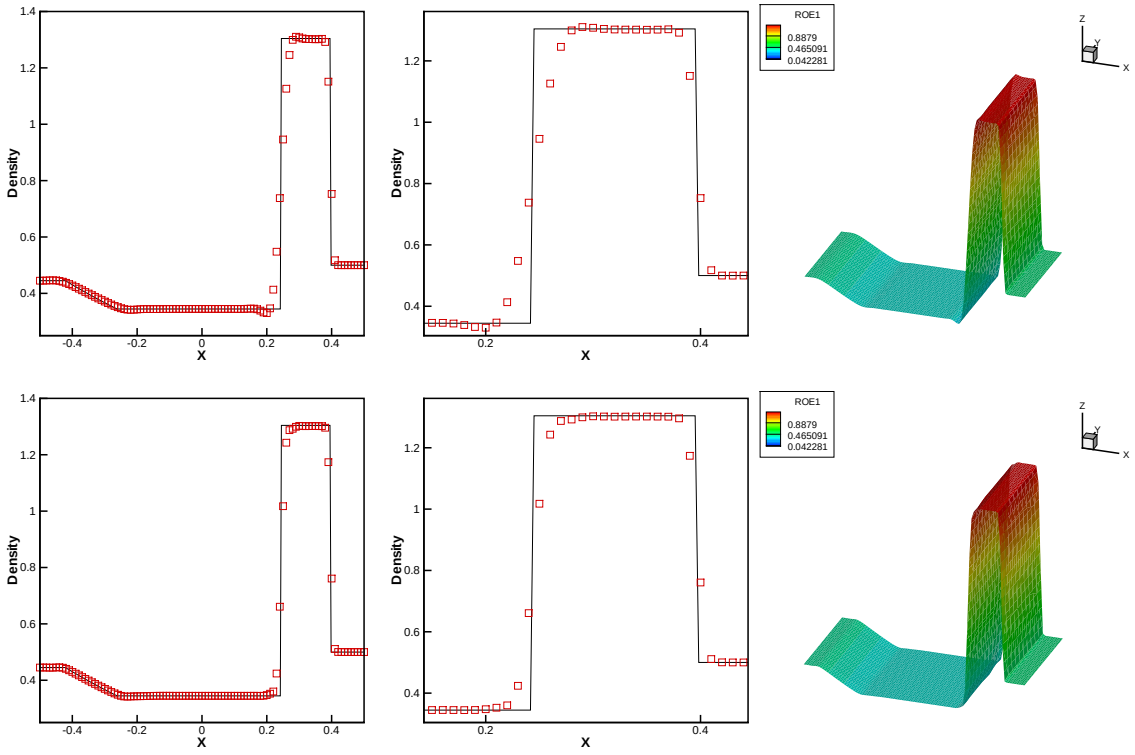

Figure 4.3: The Lax problem. T=0.16. From left to right: density; density zoomed in; 3D density surface. Solid line: the exact solution; squares: the results of WENO schemes. Top: the third order WENO scheme; bottom: the fourth order WENO scheme. The mesh points on the boundary are uniformly distributed with cell length $h = 1/100$.

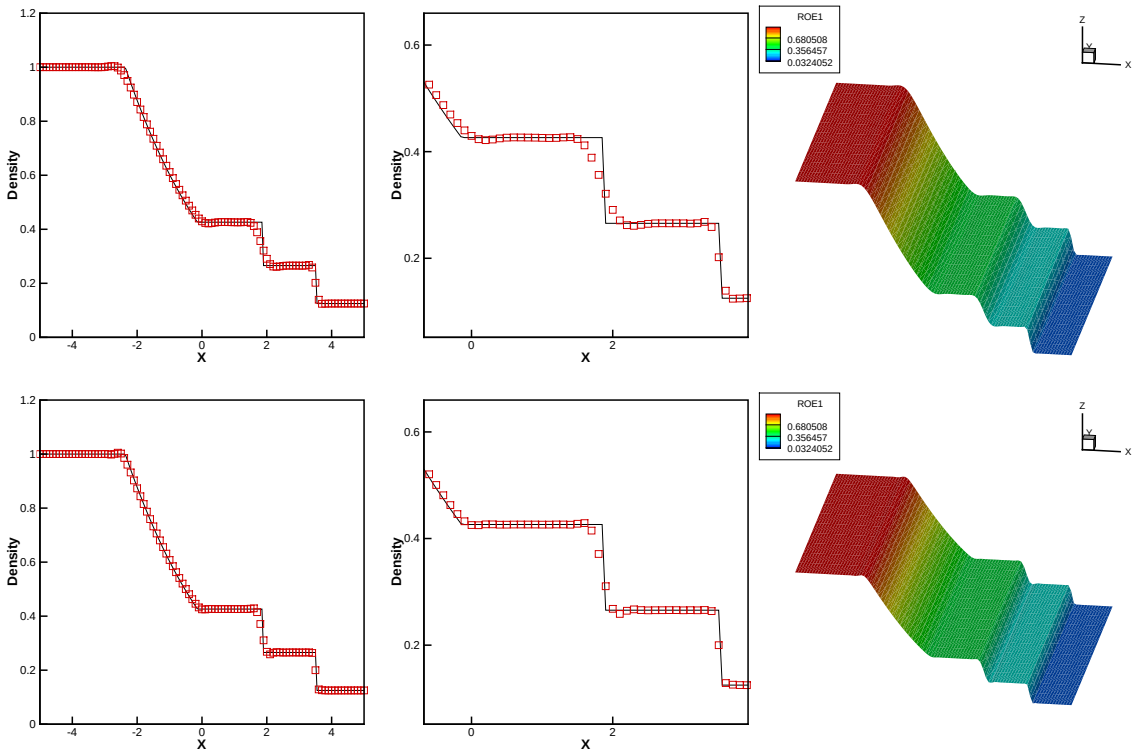

Figure 4.4: The Sod problem. T=2. From left to right: density; density zoomed in; 3D density surface. Solid line: the exact solution; squares: the results of WENO schemes. Top: the third order WENO scheme; bottom: the fourth order WENO scheme. The mesh points on the boundary are uniformly distributed with cell length $h = 1/100$.

are good for this one dimensional test example.

Example 4.5. A higher order scheme would show its advantage when the solution contains both shocks and complex smooth region structures. A typical example for this is the problem of shock interaction with entropy waves [21]. We solve the Euler equations (4.2) with a moving Mach=3 shock interacting with sine waves in density in x direction: $(\rho, \mu, \nu, p)^T = (3.857143, 2.629369, 0, 10.333333)^T$ for $x \in [-5, -4)$; $(\rho, \mu, \nu, p)^T = (1 + 0.2\sin(5x), 0, 0, 1)^T$ for $x \in [-4, 5]$. The solution of the Euler equations (4.2) in the domain of $[-5, 5] \times [-5\triangle x, 5\triangle x]$ with a triangulation of 401 vertices in the x direction and 11 vertices in the y direction. The periodic boundary condition is applied in the y direction. The computed density ρ is plotted at $t = 1.8$ against the referenced "exact" solution which is a converged solution computed by the finite difference fifth order WENO scheme [13] with

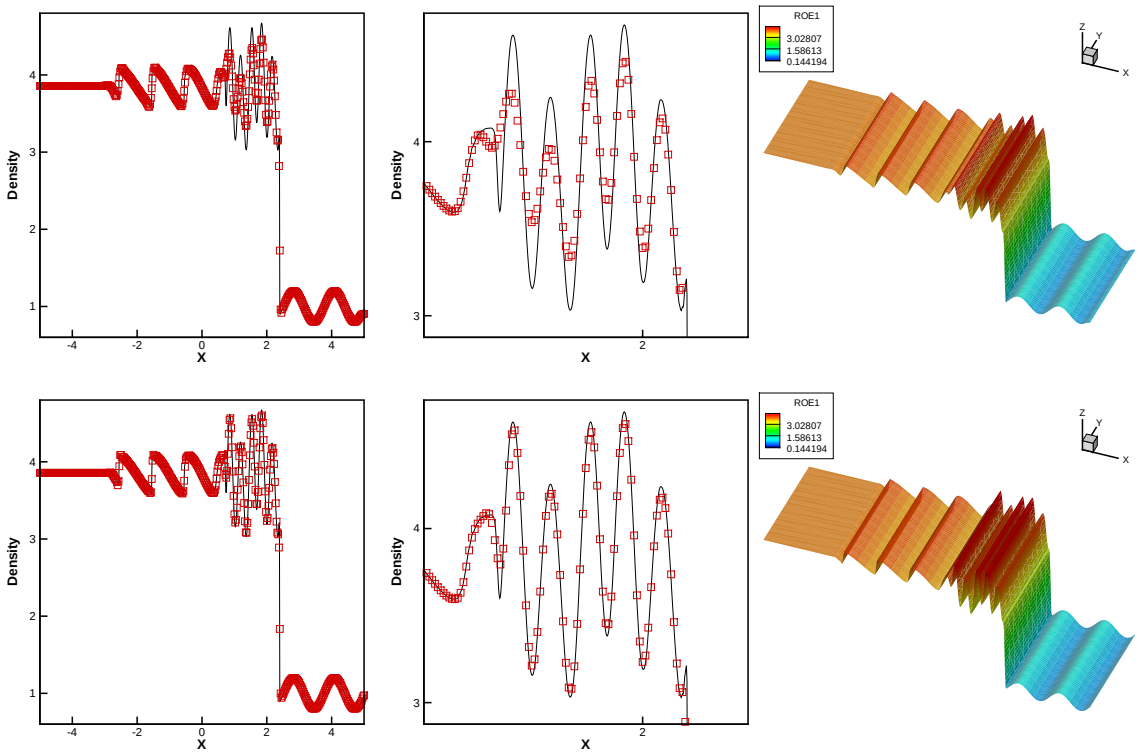

Figure 4.5: The shock density wave interaction problem. T=1.8. From left to right: density; density zoomed in; 3D density surface. Solid line: the exact solution; squares: the results of WENO schemes. Top: the third order WENO scheme; bottom: the fourth order WENO scheme. The mesh points on the boundary are uniformly distributed with cell length $h = 1/400$.

2000 grid cells in Figure 4.5. The new type of finite volume WENO schemes could get good resolution for this benchmark example.

Example 4.6. We now consider the interaction of two blast waves. The initial conditions are:

$$(\rho, \mu, \nu, p)^T = \begin{cases} (1, 0, 0, 10^3)^T, & 0 < x < 0.1, \\ (1, 0, 0, 10^{-2})^T, & 0.1 < x < 0.9, \\ (1, 0, 0, 10^2)^T, & 0.9 < x < 1. \end{cases} \tag{4.5}$$

The computed density ρ is plotted at t=0.038 against the reference "exact" solution which is a converged solution computed by the finite difference fifth order WENO scheme [13] with 2000 grid cells in Figure 4.6. The solution of the Euler equations (4.2) in the domain of $[0, 1] \times [-5\triangle x, 5\triangle x]$ with a triangulation of 401 vertices in the x direction and 11 vertices in the y direction. The periodic boundary condition is applied in the y direction. The results

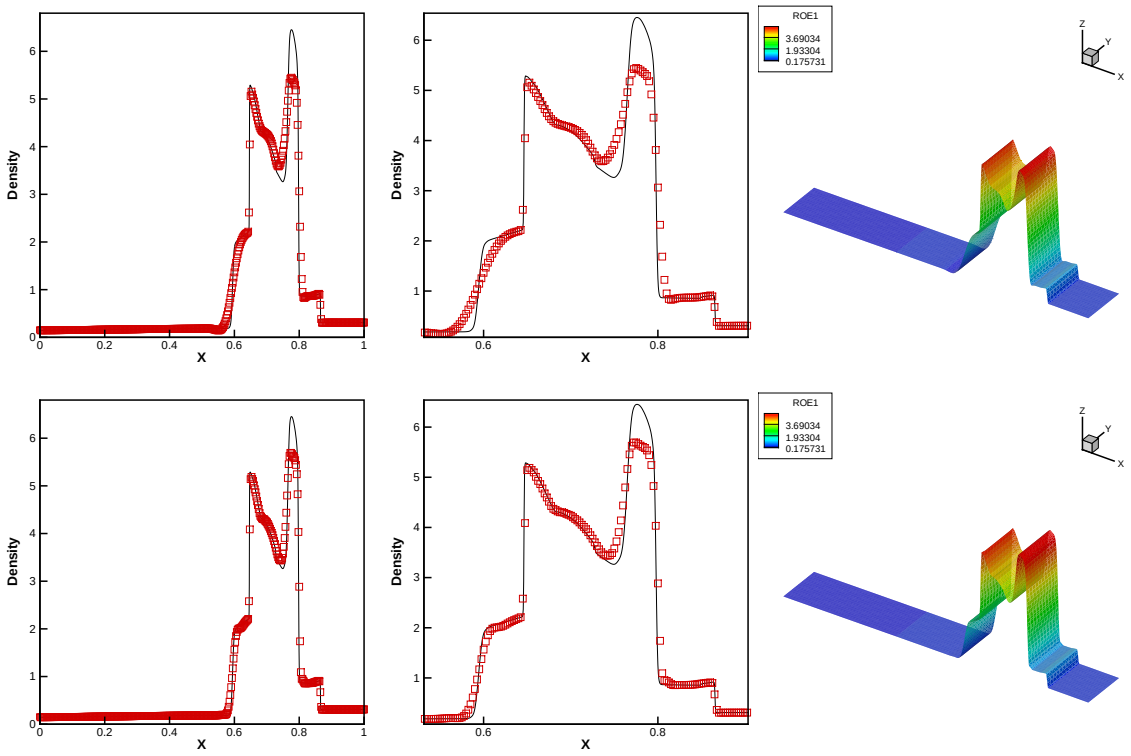

Figure 4.6: The blast wave problem. T=0.038. From left to right: density; density zoomed in; 3D density surface. Solid line: the exact solution; squares: the results of WENO schemes. Top: the third order WENO scheme; bottom: the fourth order WENO scheme. The mesh points on the boundary are uniformly distributed with cell length $h = 1/400$.

and zoomed in picture for different schemes are shown in Figure 4.6. The new WENO schemes could get good performance as before.

Example 4.7. We solve the same two dimensional Burgers equation (4.1) with the same initial condition $\mu(x, y, 0) = 0.5 + \sin(\pi(x + y)/2)$, except that the results are plotted at $t = 1.5/\pi$ when a shock has already appeared in the computational domain. The solutions are shown in Figure 4.7. We can see that the new schemes give non-oscillatory shock transitions nearby discontinuities sharply without considering the mesh's geometry which is crucial to confine associated nonnegative linear weights [19].

Example 4.8. Double Mach reflection problem. This model problem is originally from [26]. We solve the Euler equations (4.2) in a computational field $[0, 4] \times [0, 1]$. The reflection boundary condition is used at the wall, which for the rest of the bottom boundary (the part

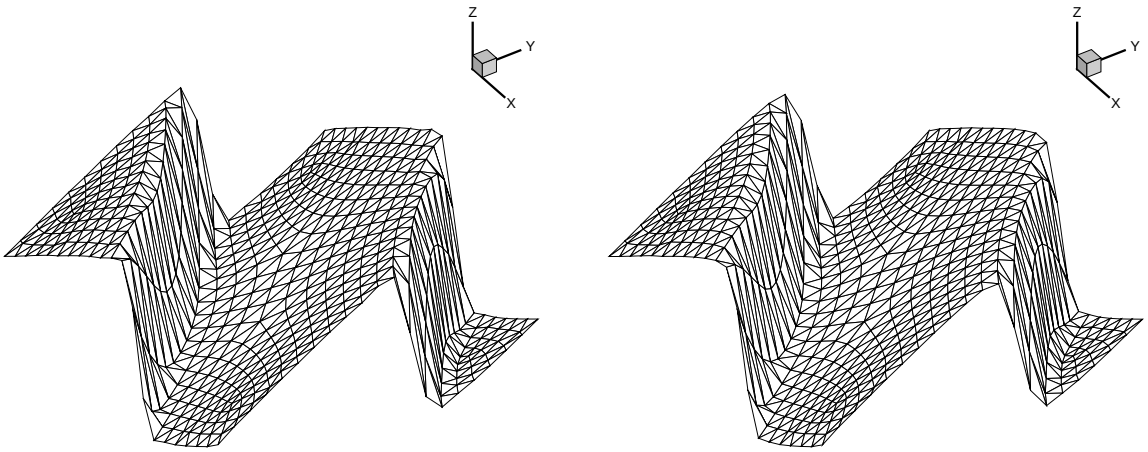

Figure 4.7: Burgers equation. $T = 1.5/\pi$. The surface of the solution. Left: the third order WENO scheme; right: the fourth order WENO scheme. The mesh points on the boundary are uniformly distributed with cell length $h = 4/20$.

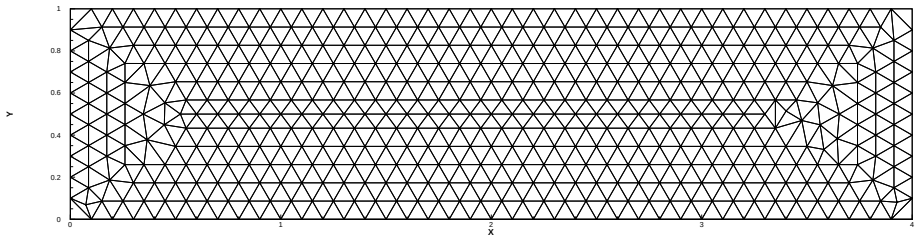

Figure 4.8: Double Mach reflection problem. Sample mesh.

from $x = 0$ to $x = \frac{1}{6}$), the exact post-shock condition is imposed. At the top boundary is the exact motion of the Mach 10 shock. The results shown are at $t = 0.2$. Two different orders of finite volume WENO schemes are used in this numerical experiment. A sample mesh coarser than what is used is shown in Figure 4.8. The simulation results are shown in Figure 4.9. The zoomed in pictures around the double Mach stem to show more details are given in Figure 4.10. We could get perfect results once again.

Example 4.9. A Mach 3 wind tunnel with a step. This model problem is also originally from [26]. The setup of the problem is as follows. The wind tunnel is 1 length unit wide and 3 length units long. The step is 0.2 length units high and is located 0.6 length units from

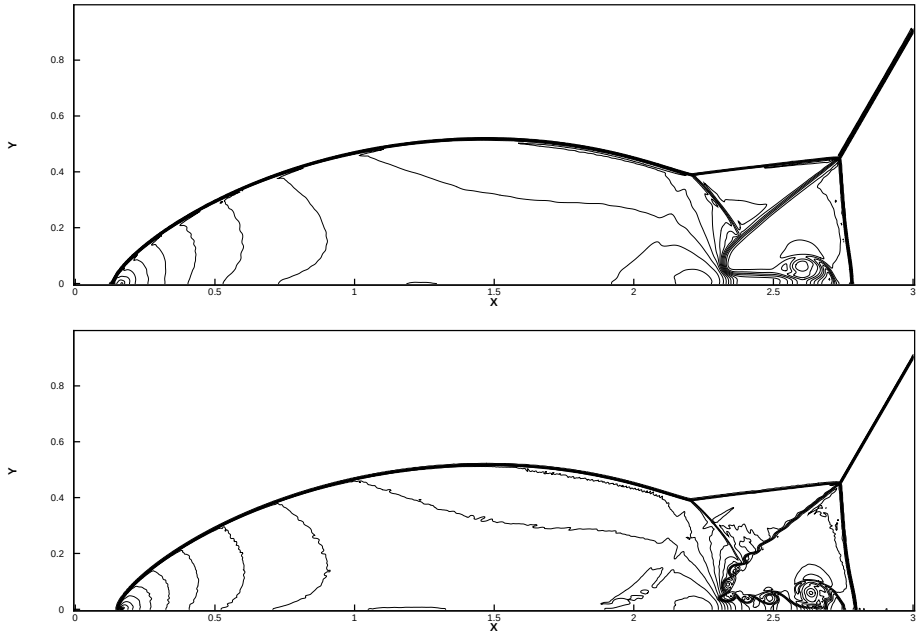

Figure 4.9: Double Mach reflection problem. 30 equally spaced density contours from 1.5 to 22.7. Top: the third order WENO scheme; bottom: the fourth order WENO scheme. The mesh points on the boundary are uniformly distributed with cell length $h = 1/320$.

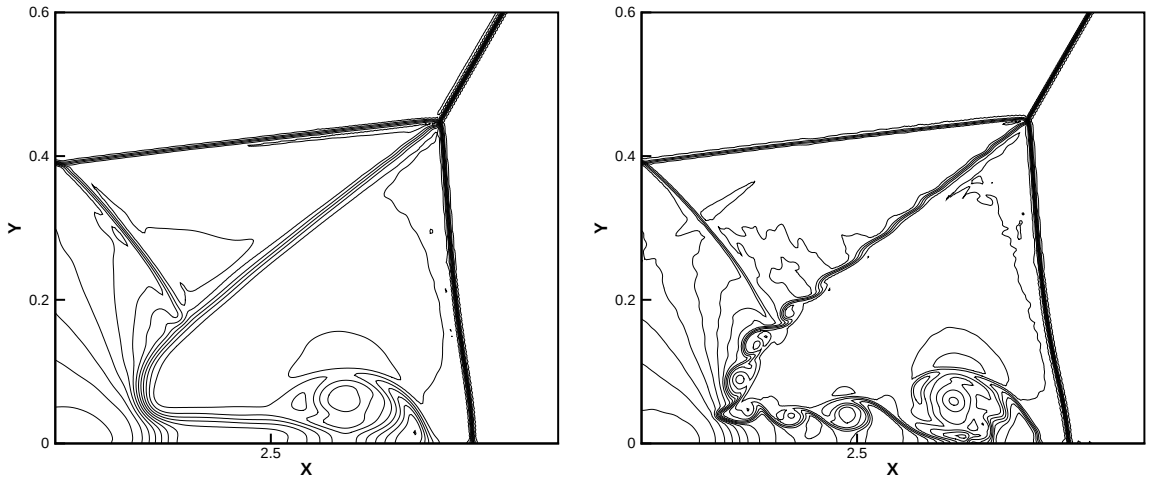

Figure 4.10: Double Mach reflection problem. Zoomed in pictures around the Mach stem. 30 equally spaced density contours from 1.5 to 22.7. Left: the third order WENO scheme; right: the fourth order WENO scheme. The mesh points on the boundary are uniformly distributed with cell length $h = 1/320$.

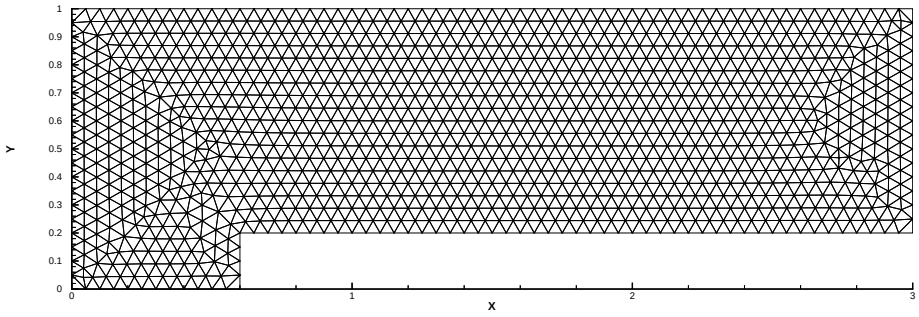

Figure 4.11: Forward step problem. Sample mesh.

the left-hand end of the tunnel. The problem is initialized by a right-going Mach 3 flow. Reflective boundary conditions are applied along the wall of the tunnel and inflow/outflow boundary conditions are applied at the entrance/exit. At the corner of the step, there is a singularity. However we do not modify our schemes or refine the mesh near the corner, in order to test the performance of our schemes for such singularity. The results are shown at $t = 4$. A sample mesh coarser than what is used is shown in Figure 4.11. And in Figure 4.12, we show 30 equally spaced density contours from 0.32 to 6.15 computed by the third order and fourth order WENO schemes. We can clearly observe that the fourth order scheme gives better resolution than the third order scheme, especially for the resolution of the physical instability and roll-up of the contact line.

Example 4.10. We consider inviscid Euler transonic flow past a single NACA0012 airfoil configuration with Mach number $M_\infty = 0.8$, angle of attack $\alpha = 1.25^\circ$ and with $M_\infty = 0.85$, angle of attack $\alpha = 1^\circ$. The computational domain is $[-15, 15] \times [-15, 15]$. The mesh used in the computation is shown in Figure 4.13, consisting of 9340 elements with the maximum diameter of the circumcircle being 1.4188 and the minimum diameter being 0.0031 near the airfoil. The third order and fourth order WENO schemes are used in the simulations. Mach number and pressure distributions are shown in Figure 4.14. And then the reductions of density residual as a function of the number of iterations are shown in Figure 4.15 and Figure 4.16, respectively. We can see that the fourth order WENO scheme has better resolution than the third order one and both of them could maintain good convergence property for

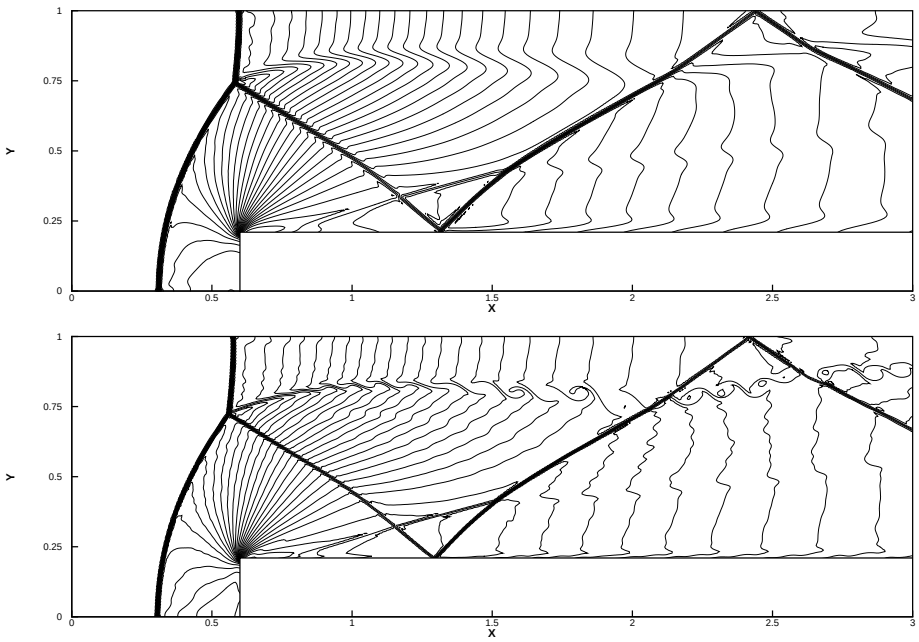

Figure 4.12: Forward step problem. 30 equally spaced density contours from 0.32 to 6.15. Top: the third order WENO scheme; bottom: the fourth order WENO scheme. The mesh points on the boundary are uniformly distributed with cell length $h = 1/160$.

this benchmark problem.

5 Concluding remarks

In this paper we investigate using a new type of third order and fourth order finite volume WENO schemes on triangular meshes. The main advantages of the new WENO schemes are their easy implementation on unstructured meshes, compact property, the application of less number of unequal size spatial stencils [32, 33] and could obtain high order accuracy in smooth region simultaneously maintaining shock transitions sharply without redundantly considering the quality of the computational meshes. It is easy for us to get one big stencil and four small stencils containing ten cells distinctly, use the information defined on associated five unequal stencils to construct a quadratic or cubic polynomial and four linear polynomials in a least square sense, modify the high degree polynomial by subtracting four linear polynomials with suitable positive constants for the sake of canceling lower degree polynomials' contributions in smooth region, decrease the effectiveness of distorted geome-

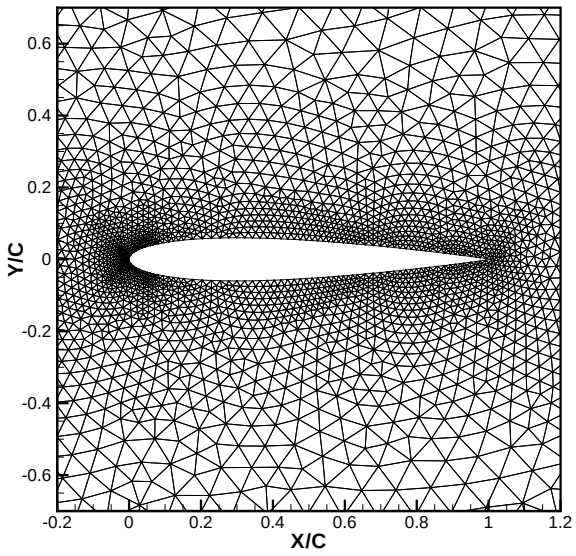

Figure 4.13: NACA0012 airfoil. Sample mesh, zoomed in.

tries of the computing meshes and reduce the difficulty in computing the linear systems for solving the linear weights at different quadrature points by means of designing a new linear weights choosing principle. So it is a promising method that could be easily extended to perform adaptive calculations, moving mesh simulations, arbitrary Lagrangian-Eulerian methods and so on.

References

[1] R. Abgrall, On essentially non-oscillatory schemes on unstructured meshes: Analysis and implementation, J. Comput. Phys., 114 (1993), 45-58.

[2] R. Borges, M. Carmona, B. Costa and W.S. Don, An improved weighted essentially non-oscillatory scheme for hyperbolic conservation laws, J. Comput. Phys., 227 (2008), 3191-3211.

[3] J. Casper, Finite-volume implementation of high-order essentially nonoscillatory schemes in two dimensions, AIAA Journal, 30 (1992), 2829-2835.

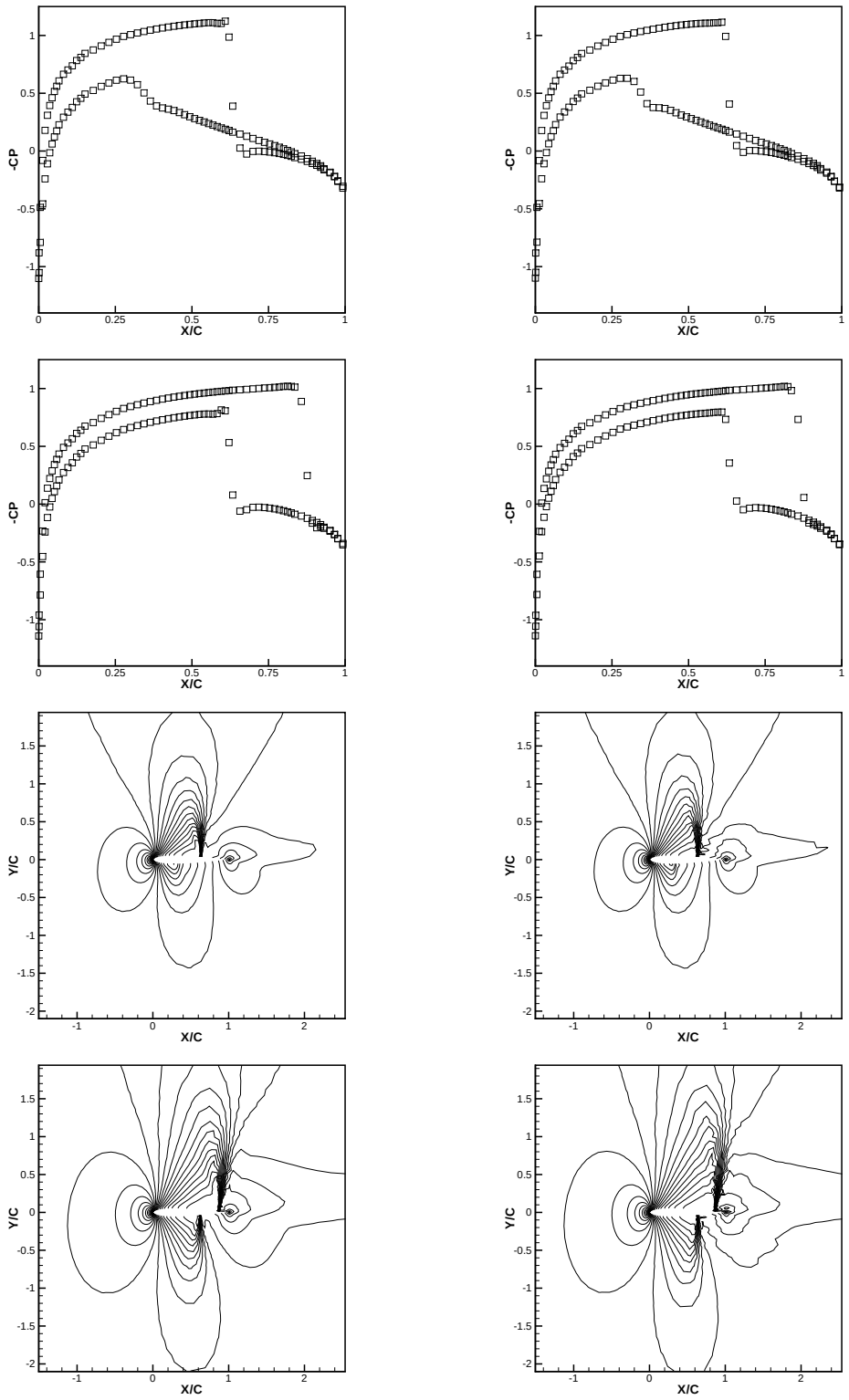

Figure 4.14: NACA0012 airfoil. From top to bottom: $M_\infty = 0.8$, angle of attack $\alpha = 1.25°$, pressure distribution; $M_\infty = 0.85$, angle of attack $\alpha = 1°$, pressure distribution; $M_\infty = 0.8$, angle of attack $\alpha = 1.25°$, 30 equally spaced mach number contours from 0.172 to 1.325; $M_\infty = 0.85$, angle of attack $\alpha = 1°$, 30 equally spaced mach number contours from 0.158 to 1.357. Left: the third order WENO scheme; right: the fourth order WENO scheme.

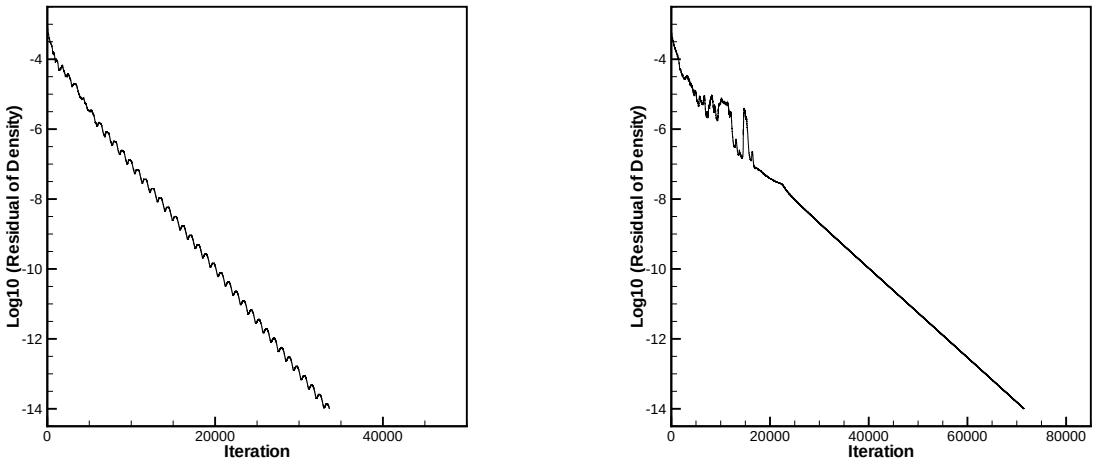

Figure 4.15: NACA0012 airfoil. $M_\infty = 0.8$, angle of attack $\alpha = 1.25°$. Reduction of density residual as a function of the number of iterations. Left: the third order WENO scheme; right: the fourth order WENO scheme.

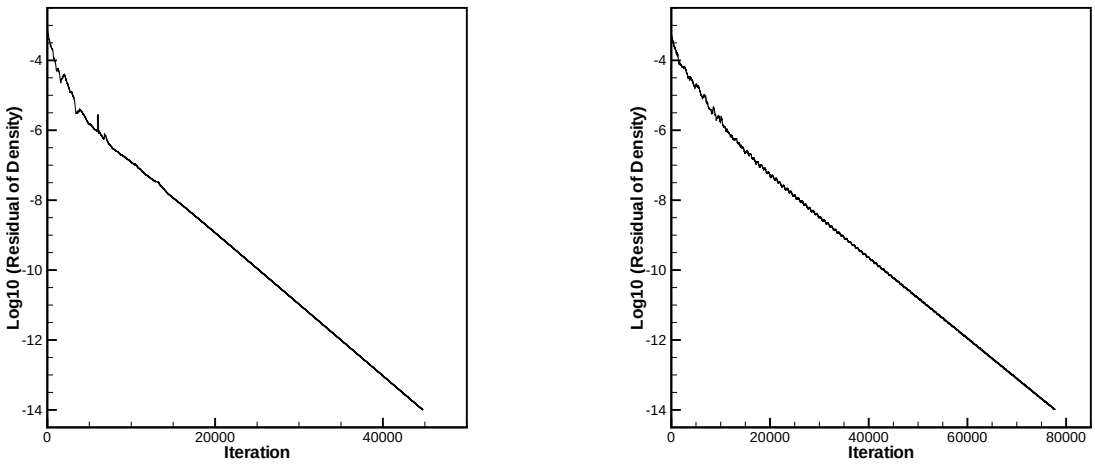

Figure 4.16: NACA0012 airfoil. $M_\infty = 0.85$, angle of attack $\alpha = 1°$. Reduction of density residual as a function of the number of iterations. Left: the third order WENO scheme; right: the fourth order WENO scheme.

[4] J. Casper and H.-L. Atkins, A finite-volume high-order ENO scheme for two-dimensional hyperbolic systems, J. Comput. Phys., 106 (1993), 62-76.

[5] M. Castro, B. Costa and W.S. Don, High order weighted essentially non-oscillatory WENO-Z schemes for hyperbolic conservation laws, J. Comput. Phys., 230 (2011), 1766-1792.

[6] M. Dumbser and M. Käser, Arbitrary high order non-oscillatory finite volume schemes on unstructured meshes for linear hyperbolic systems, J. Comput. Phys., 221 (2007), 693-723.

[7] M. Dumbser, M. Käser, V.A. Titarev, E.F. Toro, Quadrature-free non-oscillatory finite volume schemes on unstructured meshes for nonlinear hyperbolic systems, J. Comput. Phys., 226 (2007), 204-243.

[8] O. Friedrichs, Weighted essentially non-oscillatory schemes for the interpolation of mean values on unstructured grids, J. Comput. Phys., 144 (1998), 194-212.

[9] A. Harten, Preliminary results on the extension of ENO schemes to two-dimensional problems, in Proceedings, International Conference on Nonlinear Hyperbolic Problems, Saint-Etienne, 1986, Lecture Notes in Mathematics, edited by C. Carasso *et al.* (Springer-Verlag, Berlin, 1987), pp. 23-40.

[10] A. Harten and S.R. Chakravarthy, Multi-dimensional ENO schemes for general geometries ICASE Report (1991), 91-76.

[11] A. Harten, B. Engquist, S. Osher and S. Chakravathy, Uniformly high order accurate essentially non-oscillatory schemes, III, Journal of Computational Physics, 71 (1987), 231-303.

[12] C. Hu and C.-W. Shu, Weighted essentially non-oscillatory schemes on triangular meshes, Journal of Computational Physics, 150 (1999), 97-127.

[13] G. Jiang and C.-W. Shu, Efficient implementation of weighted ENO schemes, Journal of Computational Physics, 126 (1996), 202-228.

[14] D. Levy, G. Puppo and G. Russo, Central WENO schemes for hyperbolic systems of conservation laws, Mathematical Modelling and Numerical Analysis (M^2AN), 33 (1999), 547-571.

[15] X. Liu, S. Osher and T. Chan, Weighted essentially non-oscillatory schemes, Journal of Computational Physics, 115 (1994), 200-212.

[16] Y. Liu and Y.T. Zhang, A robust reconstruction for unstructured WENO schemes, Journal of Scientific Computing, 54 (2013), 603-621.

[17] J. Qiu and C.-W. Shu, On the construction, comparison, and local characteristic decomposition for high order central WENO schemes, Journal of Computational Physics, 183 (2002), 187-209.

[18] J. Qiu and C.-W. Shu, Hermite WENO schemes and their application as limiters for Runge-Kutta discontiuous Galerkin method II: two dimensional case, Computers & Fluids, 34 (2005), 642-663.

[19] J. Shi, C. Hu and C.-W. Shu, A technique of treating negative weights in WENO schemes, Journal of Computational Physics, 175 (2002), 108-127.

[20] T. Sonar, On the construction of essentially non-oscillatory finite volume approximations to hyperbolic conservation laws on general triangulations: Polynomial recovery, accuracy and stencil selection, Comput. Methods Appl. Mech. Engrg., 140 (1997), 157-181.

[21] C.-W. Shu, Essentially non-oscillatory and weighted essentially non-oscillatory schemes for hyperbolic conservation laws, in *Advanced Numerical Approximation of Nonlinear*

Hyperbolic Equations, edited by A. Quarteroni, Editor, Lecture Notes in Mathematics, CIME subseries (Springer-Verlag, Berlin/New York); ICASE Report 97-65.

[22] C.-W. Shu and S. Osher, Efficient implementation of essentially non-oscillatory shock-capturing schemes, Journal of Computational Physics, 77 (1988), 439-471.

[23] C.-W. Shu and S. Osher, Efficient implementation of essentially non-oscillatory shock capturing schemes II, Journal of Computational Physics, 83 (1989), 32-78.

[24] V.A. Titarev, P. Tsoutsanis, D. Drikakis, WENO schemes for mixed-element unstructured meshes, Commun. Comput. Phys., 8 (2010), 585-609.

[25] P. Vankeirsbilck, Algorithmic developments for the solution of hyperbolic conservation laws on adaptive unstructured grids, Ph.D. Thesis, Katholieke Universiteit Leuven, Faculteit Toegepaste Wetenschappen, Afdeling Numerieke Analyse en Toegepaste Wiskunde, Celestijnenlaan 2OOA, 3001 Leuven (Heverlee) 1993.

[26] P. Woodward and P. Colella, The numerical simulation of two-dimensional fluid flow with strong shocks, Journal of Computational Physics, 54 (1984), 115-173.

[27] Y.T. Zhang and C.-W. Shu, Third order WENO scheme on three dimensional tetrahedral meshes, Commun. Comput. Phys., 5 (2009), 836-848.

[28] X. Zhong and C.-W. Shu, A simple weighted essentially nonoscillatory limiter for Runge-Kutta discontinuous Galerkin methods, J. Comput. Phys., 232 (2013), 397-415.

[29] J. Zhu and J. Qiu, A new fifth order finite difference WENO scheme for solving hyperbolic conservation laws, J. Comput. Phys., 318 (2016), 110-121.

[30] J. Zhu and J. Qiu, A new type of finite volume WENO schemes for hyperbolic conservation laws, submitted to J. Sci. Comput.

[31] J. Zhu, J. Qiu, C.-W. Shu and M. Dumbser, Runge-Kutta discontinuous Galerkin method using WENO limiters II: Unstructured Meshes, Journal of Computational Physics, 227 (2008), 4330-4353.

[32] J. Zhu and N. Zhao, A kind of MWENO scheme and its applications, Acta Aerodynamica Sinica, 23 (2005), 330-333, (in chinese).

[33] J. Zhu, N. Zhao and H.S. Zheng, A kind of MWENO spectral volume (SVMWENO5) scheme, Acta Aerodynamica Sinica, 24 (2006), 331-334, (in chinese).